www.czasopisma.pan.pl PAN www.journals.pan.pl
Opto-Electronics Review 28 (2020) 8-14

PAN POLISH ACADEMY OF SCIENCES

Opto-Electronics Review

journal homepage: http://journals.pan.pl/opelre

First principle analysis of electronic, optical and thermoelectric characteristics of $XBiO_3$ (X = Al, Ga, In) perovskites

Q. Mahmood[a,b*], S. A. Rouf [c], E. Algrafy[a,b], G. Murtaza[d], S. M. Ramay[e**], A. Mahmood[f]

[a]Department of Physics, College of Science, Imam Abdulrahman Bin Faisal University, P.O. Box 1982, 31441, Dammam, Saudi Arabia
[b]Basic and Applied Scientific Research Center, Imam Abdurrahman Bin Faisal University, P.O. Box 1982, 31441, Dammam, Saudi Arabia
[c]Department of Physics, Division of Science and Technology, University of Education, Lahore, Pakistan
[d]Center for Advance Studies in Physics, GC University Lahore, Pakistan
[e]Physics and Astronomy Department, College of Science, King Saud University P.O. Box 2455, Riyadh 11451, Saudi Arabia
[f]Chemical Engineering Department, College of Engineering, King Saud University Riyadh, Saudi Arabia

Article info

Article history:
Received 19 Dec. 2019
Received in revised form 03 Feb. 2020
Accepted 28 Feb. 2020

Keywords:
DFT; Structural stability; Optoelectronics; Thermoelectric applications; Indirect band gap semiconductors

Abstract

The perovskites $XBiO_3$ (X = Al, Ga, In) have been studied in terms of mechanical, optical and thermoelectric behavior for energy harvesting application. Density functional theory is applied to study electronic, optical and thermoelectric properties of the studied materials. Structural, mechanical and thermodynamic stabilities are confirmed from the tolerance factor, Born mechanical stability and formation energy/specific heat capacity. Poisson and Plough ratios show the studied materials are ductile and have ability to withstand pressure. Band structure analysis shows the indirect band gap 3.0/2.1/1.0 eV for ABO/GBO/IBO. A complete set of optical spectra is reported by dielectric constants, refractive index, optical conduction, absorption of light and optical loss energy. Shifting of maximum absorption band to visible region increases the potential of perovskites $XBiO_3$. Transport characteristics are also investigated by electrical conductivity, Seebeck coefficient and figure of merit.

1. Introduction

In the global world the requirement of energy increase and resources become so limited that instigates the researchers to discover new sources of energy which must be cost effective, friendly to handle and nontoxic. Solar is the leading energy source among all others and its performance depends upon materials used to fabricate optoelectronic devices. The search for potential materials is a key motivation of the scientists and an extensive research has been done to achieve this goal. In the last few decades, the perovskites ceramics having formula ABO_3 gained a lot of attention due to their interesting properties suitable for the development of energy storage devices [1,2]. The perovskites oxides are extensively used for optoelectronic, thermoelectric, ferroelectric, high dielectric capacitors, ferroelectric random access memories, generators and refrigerators [3]. Among all the studied compounds, the lead based perovskites like PbTiO3, $PbZrO_3$, $BaPbO_3$, etc. are vastly in applications because of high Curie temperature, large polarization, high electrical conductivity, high energy conversion efficiency, but the major challenge with these materials is the toxic nature of lead which cannot be ignored while device fabricating. Therefore, a lot of lead- free perovskites is studied for optical and thermoelectric applications like optoelectronic and transport characteristics of $BiAlO_3$, $BaGeO_3$, $MgZrO_3$, $BiBO_3$, etc. [4].

Performance of materials for thermoelectric applications is widely predicted from the figure of merit as $ZT = S^2\sigma T/k$, where T is the kelvin temperature. Thermal conductivity of the material is contributed by electrons k_{el} and lattice vibration k_{ph} [5]. Wunderlich *et al.* [6] studied $NaTaO_3$ to highlight its potential for thermoelectric applications. It was known previously [7-9] that doping of nonmetals or metals mostly reduces the energy band gap of semiconductor oxides. It also shifts the wavelength to visible region resulting in useful thermoelectric and optical

*Corresponding author email; Q. Mahmood qmmustafa@iau.edu.sa; tel. 00966567158351; **S. M Ramay schaudhry@ksu.edu.sa

https://doi.org/10.24425/opelre.2020.132497

properties. Sfirloaga *et al*. [10] doped Fe or Ag in $NaTaO_3$ which decreases the energy bandgap by 1 - 2 eV. It was observed that decrease in bandgap increases electric conductivity and Seebeck coefficient. It was concluded in Ref. 8 that these doped $NaTaO_3$ materials are potential candidates for thermoelectric applications. Many researchers [11-13] have studied the electronic properties of K doped $BaBiO_3$ to study metallicity at ambient conditions [14]. There are many other perovskite oxides such as $SrTiO_3$ and $CaMnO_3$, as well as ZnO which were identified as potential n-type thermoelectric materials [15-17].

In light of the above literature we have computed electronic properties from band structures, optical properties from tensor matrix and transport properties from Boltzmann theory of perovskites $XBiO_3$ (where X = Al, Ga and In) in the frame work of Wien2k code [18]. The studied perovskites optoelectronic characteristics are investigated dielectric constants, refractive index, reflectivity and absorption coefficient. Transport characteristics are explored by Weidman-Franz law and figure of merit. The limited theoretical and experimental literature on $XBiO_3$ compounds exist. Therefore, our theoretical prediction will facilitate the experimentalists to explore them for device fabrication.

2. Calculations' details

The cubic structures of ABO/GBO/IBO (221-Pm3m) are optimized by PBE-GGA [19]. These approximations are incorporated in the full potential linearized augmented plane wave method which is developed in the Wien2k code [18]. The ground states parameters like lattice constant a_o, bulk modulus *B* and ground states energy are calculated by Murnaghan equation. To calculate the band gap dependent optical and thermoelectric properties, the electronic structures' energy/charge is converged through self-consistent field by PBE-GGA and TB-mBJ potential [20]. The PBE-GGA approximates the ground state properties accurately but underestimates the band gap. We have implemented the TB-mBJ potential to improve band gap. The wave vector in reciprocal lattice and radius of muffin-tin sphere (core region) is multiplied to induce the constant 8. The most important for convergence analysis is the k-mesh scheme which is shown best for 10x10x10 order because the energy liberated becomes constant for this order. Furthermore, the characterizations are analyzed through different methods. The mechanical properties are calculated by the analysis of tensor matrix through Chapin method [21] to find the coefficients of nonlinear first order differential equations. For cubic symmetry (C_{11}, C_{12} and C_{44}) they are enough to illustrate mechanical behavior of the studied materials. The optical properties are analyzed through Kramers-Kronig relation [22] between dielectric constants and all the necessary parameters like refractions, absorption, reflections, etc. which are calculated from the dielectric constants. The transport characteristics are investigated by BoltzTraP code [23].

3. Results' analysis

3.1. The stability and mechanical properties

For device reliability it should be stable, therefore, the stabilities are examined by Goldschmidt tolerance factor (structural), mechanical stability (elastic constants) and thermodynamic stability (formation energy). The enthalpy of formation has been computed by the relation:

$$\Delta H_f = E_{Total}(\mathrm{X_lBi_mO_n}) - lE_X - mE_{Bi} - nE_{O,} \quad (1)$$

where $E_{Total}(X_lBi_mO_n), E_X$, E_{Bi} and E_O are the total energy and individual energies of the suitable elements. The calculated values are reported in Table 1. The negative sign of energy liberated shows that the individual elements have more energy than compound which shows stability of the studied materials [24,25]. Furthermore, structural stability has been judged by Goldschmidt equation which is calculated by the relation $t = (r_X + r_O)/\sqrt{2}(r_{Bi} + r_O)$ here r_X, r_{Bi} and r_O are the atomic radii of the cation (tetrahedral position), anion (octahedral position) and oxygen atoms. The range of tolerance factor for stability in cubic perovskites is of 0.94 to 1.02 (Table 1) [26-28]. Therefore, the structures of $XBiO_3$ perovskites are stable. Furthermore, the mechanical stability has been ensured from positive elastic constants and conditions in Ref. 29. The studied materials become less stiff when we replace cations Al with Ga and In and lattice constant increases due to an increase of interatomic distance. Poisson ratio υ and Pugh's ratio *B/G* both decide about the brittle and ductile behavior of the studied materials whose limiting cases for ductile nature are υ>0.26 and *B/G*>1.75 [30]. The calculated data ensure ductile behavior of $XBiO_3$. Further

Table 1

Properties [unit]	$AlBiO_3$	Others	$GaBiO_3$	Others	$InBiO_3$
a_o [Å]	3.79	3.78	3.89		4.17
B [GPa]	202.8		183.9		157.3
H_f [eV]	-2.44	-2.44	-1.74		-1.35
T_f	1.02		0.99		0.97
$Eg_{(X-\Gamma)}$ [eV]	3.0	1.58	2.2	1.23	1.0
$\varepsilon_1(0)$	5.4		6.1		7.5
n(0)	2.3		2.5		2.7
R(0)	0.16		0.18		0.22

The calculated lattice constant a_o (Å); Bulk modulus B_o (GPa); Formation energy H_f (eV); Tolerance factor (T_f); Band gap $Eg_{(X-\Gamma)}$ (eV), Static real dielectric constant $\varepsilon_1(0)$; Static refractive index *n(0)*; Zero frequency Reflectivity *R(0)* of $AlBiO_3$, $GaBiO_3$ and $InBiO_3$ in cubic phase by PBE-GGA and TB-mBJ potential

ductility decreases from ABO to IBO because of reducing the effect of interatomic forces. The anisotropy factor controls properties of the materials in different crystallographic axis. Its value is unity for isotropic materials and any deviation makes it anisotropic. Therefore, it is clear from Table 2, the ABO is anisotropic while IBO is an almost isotropic material.

Table 2

Properties [unit]	$AlBiO_3$	$GaBiO_3$	$InBiO_3$
C_{11} [GPa]	300	272	259
C_{12} [GPa]	151	109	95
C_{44} [GPa]	130	94	87
B [GPa]	200	163	149
G ([GPa]	103	89	84
Y [GPa]	265	225	214
B/G	1.93	1.83	1.76
υ	0.28	0.27	0.26
A	1.74	1.15	1.06

The calculated elastic constants C_{11}, C_{12} and C_{44}, bulk modulus *B*, shear modulus *G*, Young modulus *Y*, Pugh ratio (*B/G*); Poission ratio υ, anisotropy factor *A*, of AlBiO3, GaBiO3 and InBiO3 in cubic phase by PBE-GGA and TB-mBJ potential.

3.2. *Electronic Properties*

Optimized and relaxed structures are energy converged to find the basic parameters: lattice constant, bulk modulus, etc. The optimized structures' energy is plotted against volume in Figs. 1(a), 1(b) and 1(c) (right side) and their crystal structures with a cubic 1x1x1 unit cell and space group (221) Pm3m (lift side).

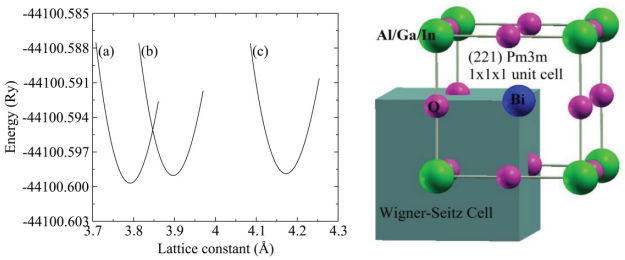

Fig. 1 The energy E *vs*. lattice constant optimized plots of (a) $AlBiO_3$, (b) $GaBiO_3$ and (c) $InBiO_3$: Crystal structure of 1x1x1 unit cell and Wigner-Seitz Cell.

The Al/Ga/In atoms are present at the corners of tetrahedron while the Bi atom at body center position is occupied by octahedron of oxygen atoms. The lattice constant increases from ABO to IBO and bulk modulus decreases by increasing atomic radius. The increasing lattice constant shifts the electronic states closer which reduces the energy gap between VB and CB as shown in Fig. 2.

The indirect band gap E_g (R-X) decreases from ABO to IBO because of a greater atomic size of In than Al. The visible region of electromagnetic spectrum for light absorption shifted from visible to infrared. To see the effect of sub-atomic states on the band gap, states' density is plotted in Fig. 3.

At valence band edge the major contribution comes from oxygen with minor contribution of Al/Ga/In and Bi

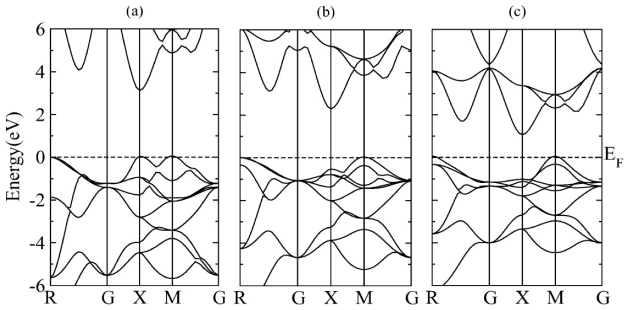

Fig. 2 The band structures of (a) AlBiO3, (b) GaBiO3 and (c) InBiO3 are calculated by TB-mBJ potential.

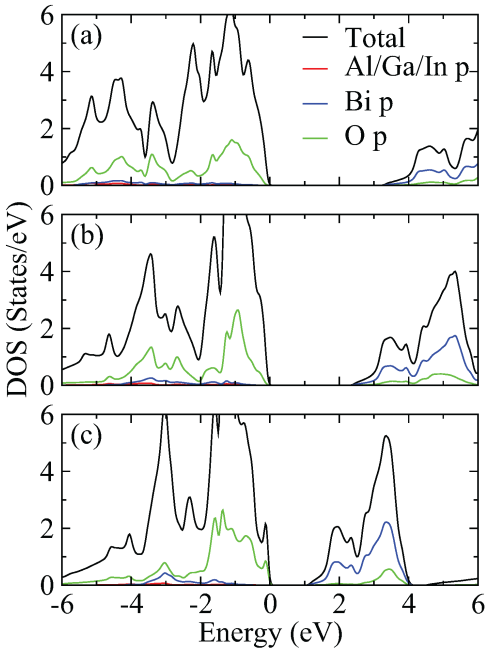

Fig. 3 The total and partial density of states of (a) AlBiO3, (b) GaBiO3 and (c) InBiO3 are calculated by TB-mBJ potential.

while at conduction band edge Bi states also contribute dominantly. The tuning of band gap by hybridization of atomic states influences the physical characteristics.

3.3. *Optical Properties*

Optical behavior of materials is based on interaction between phonons and lattice atoms. Solar cell and other optoelectronic applications demand visible region absorbs more light. Therefore, to tune the band gap, we replace the Al with Ga and In which reduces the band gap [31-34]. There are two types of transitions: inter-band and intra-band. The inter-band transitions from valence band to conduction are dominated in perovskites as compared to within the band transitions [35-36]. The complete optical analysis has been done by the dielectric constant $\varepsilon(\omega)$ = Re $\varepsilon(\omega)$ + Im $\varepsilon(\omega)$ of which Re and Im are real and imaginary identities. These identities are co-related by Kramers-Kronig relation [37-38]. The other optical properties have been calculated from the Re $\varepsilon(\omega)$ and Im $\varepsilon(\omega)$ by Refs. 39 and 40 and presented in Figs. 4(a)-4(d) and Figs. 5(a)-5(d).

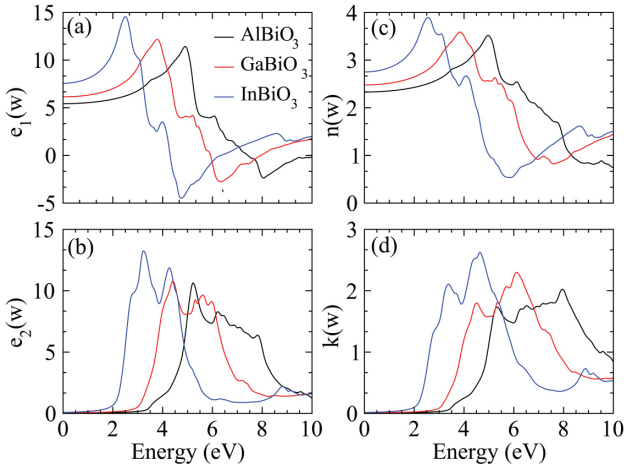

Fig. 4 (a) The real part of dielectric constant, (b) imaginary part of dielectric constant, (c) refractive index and extinction coefficient *vs*. energy plots of $AlBiO_3$, $GaBiO_3$ and $InBiO_3$.

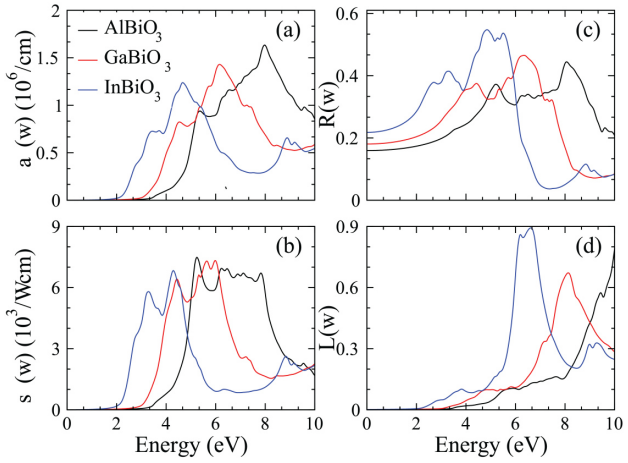

Fig. 5 (a) The absorption coefficient, (b) optical conductivity, (c) reflectivity and optical loss *vs*. energy plots of $AlBiO_3$, $GaBiO_3$ and $InBiO_3$.

Re $\varepsilon(\omega)$ is the direct measurement of how much light is scattered or plane polarized when it travels through material whose different atomic layers have different refractive index. The maximum dispersion of light occurs at resonance frequency because phase velocity of the wave depends on it as shown in Fig. 4(a). The resonance peaks of the studied materials are shifted towards high energy region of 2.50 eV/3.80 eV/4.95 eV for ABO/GBO/IBO, respectively. When the frequency slightly increases from resonance value, Re $\varepsilon(\omega)$ decreases sharply to minimum at 4.3 eV/6.0 eV/7.50 eV for ABO/GBO/IBO and approaches to negative peaks [Fig. 4(a)]. The negative values of real part of $\varepsilon(\omega)$ show metal like behavior which reflects light. Reason for the reflection of electromagnetic radiations from materials surface is zero band gap of metals which is not compatible with the photons' energy to fulfill the necessary condition for absorption. After 7 eV, Re $\varepsilon(\omega)$ again becomes positive but this energy region is not our area of concern. Furthermore, the substitution Ga/In at Al site shifts the resonance peaks towards low frequency because of addition of extra shells that reduces the electronic states' separations. The static value Re $\varepsilon(0)$ is linked with the band gap energy E_g of the studied materials through mathematical equation Re $\varepsilon(0) \approx 1+ (\hbar\omega_p/E_g)^2$ [41].

The Im $\varepsilon(\omega)$ is the measure of how much light energy material can absorb/attenuate [Fig. 4(b)]. The threshold frequency shows the band gap as 3.4 eV for ABO, 3.0 eV for GBO and 2 eV for IBO, respectively. These band gaps are overestimated band structures reported band gaps (3.0 eV/2.2 eV/1 eV for ABO/GBO/IBO) because of approximations used in density functional theory calculations and limitations of mathematical functions [42]. From critical values, Im $\varepsilon(\omega)$ increases to peaks at 3.2 eV/4.4 eV/5.2 eV for ABO/GBO/IBO, respectively. When frequency increases from resonance value of Re $\varepsilon(\omega)$ light polarization direction changes and it gets attenuated by the material. Furthermore, the attenuation band of frequency decreases from 3.4 eV (ABO) to 2.3 eV (IBO) and band gap decreases which shifts absorption region to visible. The absorption of light falls sharply at 4.7 eV/6.3 eV/8.0 eV for ABO/GBO/IBO, respectively because of negative value of Re $\varepsilon(\omega)$ that gives the metallic response and shows the consistency of calculated results through Kramers-Kronig relation. For ABO, the absorption band lies in ultraviolet region and has active applications in sterilized surgical equipment and optical remote sensing while GBO and IBO have absorption band in visible region that favors the solar cell fabrications.

Equation $V_g(nd\lambda - \lambda dn) = nd\lambda V_P$ relates to the group velocity V_g, the refractive index $n(\omega)$ and the phase velocity V_p that illustrate the materials' transparency for light. The refractive index decides in which region of electromagnetic spectrum the optical device is operational. Its value from 2 to 3 is suitable for visible light operating solar cells.

The refractive index $n(\omega)$ has same results as Re $\varepsilon(\omega)$ and connected by equation $n^2 - k^2 = Re\,\varepsilon(\omega)$ as shown in Fig. 4(c). The values at zero frequency of both Re $\varepsilon(0)$ and n(0) are satisfying equation $n_0^2 = Re\,\varepsilon(0)$. The peak values of refractive indices of ABO, GBO and IBO are of 6 eV, 3.8 eV and 2.5 eV, respectively. After the peak values at resonance, it drops monotonically and becomes fractional at 8 eV, 6 eV and 5 eV because of $V_g > C$ and materials left-handed mode which is yet not explored physically [43]. The extinction coefficient $k(\omega)$ is the replica of an imaginary part of dielectric constant and satisfies the condition $2nk(\omega)$ = Re $\varepsilon(0)$ as presented in Fig.4(d). This resemblance of these two quantities ensures the reliability of theoretically explored characteristics from the dielectric constants and refraction.

The attenuation of light has been shown by the absorption coefficient $\alpha(\omega)$ which was graphically represented in Fig.5(a). Its critical value shows optical band gaps whose numerical values are of 3 eV/2.5 eV/1.6 eV for ABO/GBO/IBO, respectively. The calculated band gap is overestimated by a small number from the band calculated by band structures because of the theoretical approximations involved. Furthermore, the maximum absorption peaks exist at energies of 8 eV/6 eV/4.5 eV for ABO/GBO/IBO, respectively. The substitution Al with Ga and In moves the absorption from ultraviolet to visible. The optical conductivity $\sigma(\omega)$ depends upon the absorption of light because light energy accelerates the electrons for conduction process. The calculated values are graphically represented in Fig.5(b) and illustrate the peaks at 4.6 eV/4.2 eV/4.0 eV for ABO/GBO/IBO perovskites. The

region between 4 eV to 8 eV shows that the fluctuation in peaks may be of different rate of electrons' holes reaction when light is exposed to material. The reflection of light increases to peak at 8 eV/6 eV/5 eV for ABO/GBO/IBO, respectively as presented in Fig.5(c). eVen though three processes: absorption, conduction and reflection take place simultaneously. The loss of optical energy through heat and dispersion is represented in Fig. 5(d) which is the minimum in visible range. Therefore, the studied perovskites are potential materials for optical device fabrications.

3.4. *Thermoelectric characterstics*

Thermal efficiency of the studied materials can be estimated by figure of merit ZT as discussed briefly in introduction. To obtain the higher value of ZT, value of parameters appearing in the nominator of ZT equation should be high and value the of parameter (i.e., the thermal conductivity) in the denominator should be small. According to the limitations of BoltzTraP code, the lattice contribution k_{ph} has been ignored and only electrons' contribution to thermal heat has been taken under consideration [44-46]. The calculated thermoelectric properties are plotted in Figs. 6(a)-6(d).

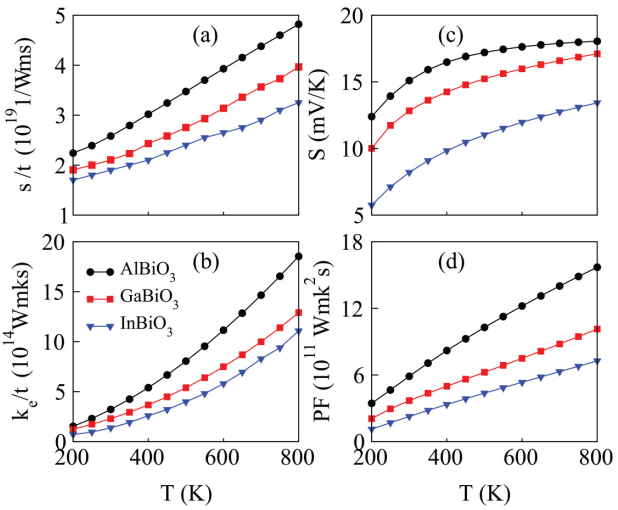

Fig. 6 (a) Electrical conductivity, (b) thermal conductivity, (c) Seebeck coefficient and (d) power factor plotted *vs.* temperature of $AlBiO_3$, $GaBiO_3$ and $InBiO_3$

The electrical conductivity increases with increasing temperature up to 800 K [Fig.6(a)]. The graphs' slopes elucidate that ABO has the highest electrical conductivity while IBO the least at the same temperature for the studied compounds because Al metal provides more free electrons as compared to Ga and In. The thermal conductivity plays an important role to decide about device efficiency because the quantized energy of elastic mechanical waves of the lattice vibration has a strong effect on it [47-49]. The graphical representation of thermal conductivity shows that its value increases with increasing temperature and reaches to $18x10^{14}$ Wmks, $13x10^{14}$ Wmks and $10x10^{14}$ Wmks for ABO, GBO and IBO at 800 K. ABO has more thermal conductivity than GBO and IBO because the oscillation of Al free electrons may increase at high temperature more than GBO and IBO. For best thermoelectric materials, κ/σ should be small which is the statement of Weidman-Franz law (LT = κ/σ) [50,51]. Therefore, the LT values for the studied compounds show that the ratio is of the order of 10^{-5} and decreases from ABO to IBO for a temperature of 300 K as shown in Table 3. That makes of an important class of ceramics for electric generators, heat sensors and refrigerators applications.

Table 3

Properties	$AlBiO_3$	$GaBiO_3$	$InBiO_3$
σ	5.88×10^{19}	5.21×10^{19}	4.55×10^{19}
κ	2.58×10^{14}	2.10×10^{14}	1.9×10^{14}
κ/σ	1.24×10^{-5}	1.09×10^{-5}	0.72×10^{-5}
η	0.56	0.78	1.0

The calculated electrical conductivity σ, thermal conductivity κ, Wiedemann-Fraz ratio κ/σ, thermoelectric efficiency η of $AlBiO_3$, $GaBiO_3$ and $InBiO_3$ in cubic phase by PBE-GGA and TB-mBJ potential.

The Seebeck coefficient is the ratio of a voltage difference between thermal contacts of the metals to temperature difference and it plays a significant role in building thermoelectric efficiency. The Seebeck coefficient increases up to 400 K at a faster rate and, then, it becomes almost constant up to 800 K because at high temperature a potential barrier is maintained by the flow of charge carriers. The potential barrier for ABO is higher than GBO and IBO due to a faster collision rate of electrons. The type of charge carriers decides if the Seebeck coefficient is negative or positive. In our calculated results, the Seebeck coefficient is a positive temperature of 200 K – 800 K which ensures the p-type semiconductors.

The figure of merit is also analyzed to see that the comparative efficiencies of the studied compounds at room temperature and calculated values are presented in Table 3. The analyses reveal that IBO has the highest figure of merit among the studied compounds. The dominant cause of increasing ZT with temperature can be illustrated by the variations in an indirect band gap with temperature through equation [52]:

$$E_g(T) = E_g(0) - \frac{\alpha T^2}{T+\beta,} \qquad (2)$$

where $E_g(T)$ and $E_g(0)$ are the band gaps energy at T and zero temperature, α and β are the constants. The relation shows that the band gap decreases by increasing the temperature that increases the figure of merit because electrical conductivity increases. In Table 3, room temperature values demonstrate that thermal to electrical conductivity ratio decreases with the replacement of cation from Al to In. Therefore, the thermal efficiency as decided from ZT increases from 0.56 to 0.78 (Al to Ga) and from 0.78 to 1.0 (Ga to In) with the variation of cation. Hence, the trends of ZT expect efficient conversion of heat into electrical energy and mainly depend upon precise calculations for ρ, κ, and *S* values. This designates that further development in calculations can give the precise measurements of ZT and improve it by the selection of more accurate models than the present system [53].

4. Conclusions

In present paper, mechanical, optical and thermoelectric behavior of perovskites $XBiO_3$ have been studied for energy harvesting application. The structural optimization, tolerance factor, enthalpy of formation and Born mechanical conditions assure the structural, thermodynamic and mechanical stabilities of the studied compounds. Indirect band gap from 3.0 eV to 1.0 eV tunes absorption to visible range from ultraviolet. Furthermore, optical loss, reflectivity and dispersion of light are less in visible range. Thermoelectric efficiency has been concluded by two parameters: thermal to electrical conductivity ratio and figure of merit. The decreasing thermal to electrical conductivity ratio and increasing figure of merit (0.58 to 1.0 at room temperature) from ABO to IBO improve the efficiency to harvest more heat energy to electrical energy. This theoretical analysis may help the experimentalists realize that for energy applications.

Acknowledgement

The authors (Shahid M. Ramay and Asif Mahmood) would like to extend their sincere appreciation to the Deanship of Scientific Research at King Saud University for funding this Research group No. RG 1435-004.

References

[1] Orera, M. V. & Merino, R. I. Ceramics with photonic and optical applications. *Bol. Soc. Esp. Ceram. Vidr* **54,** 1-10 (2015).

[2] Sołtys, M., Gorny, A., Pisarska, J. & Pisarski, W. A. Electrical and optical properties of glasses and glass-ceramics. *J. Non-Crystalline Solids* **498**, 352-363 (2018)

[3] Chentg, A., Zhig, Y. & Baa, Y. A. study of $BaTiO_3$-$BaPbO_3$ ceramic composites, *Phys. Condens. Matter*, **6**, 7921-7925 (1994).

[4] Noor, N. A., Hassan, M., Rashid, M., Alay-e-Abbas, S. M. & A. Laref. Systematic study of elastic, electronic, optical and thermoelectric properties of cubic $BiBO_3$ and $BiAlO_3$ compounds at different pressure by using ab-initio calculations. *Materials Research Bulletin* **97**, 436-443 (2018).

[5] Kim, H. S., Liu, W., Chen, G., Chu, C. W. & Rena, Z. Relationship between thermoelectric figure of merit and energy conversion efficiency. *PNAS* **112**, 8205-8210 (2015).

[6] Wunderlich, W., Mori, T. & Sologub, O. SPS-sintered $NaTaO_3$-Fe_2O_3 composite exhibits enhanced Seebeck coefficient and electric current, *Mater. Renew. Sustain. Energy* **1**, 3-21 (2014).

[7] Zhao, Y. X., Liu, D. R., Li, F. F., Yang, D. F. & Jiang, Y. S. Preparation, characterization and photocatalytic activity of N-doped $NaTaO_3$ nanocubes. *Powder Technol*. **214**, 155-160 (2011).

[8] Yang, M., Huang, X., Yan, S., Li, Z., Yu, T. & Zou, Z. Improved hydrogen eVolution activities under visible light irradiation over $NaTaO_3$ co doped with lanthanum and chromium. *Mater. Chem. Phys*. **121 (3)**, 506-510 (2010).

[9] Liu, D. R., Wei, C. D., Xue, B., Zhang, X. G. & Jiang, Y. S. Synthesis and photocatalytic activity of N-doped $NaTaO_3$ compounds calcined at low temperature. *J. Hazard. Mater*. **182,** 50-54 (2010).

[10] Sfirloaga, P., Marin, C. N., Malaescu, I. & Vlazan, P. The electrical performance of ceramics materials with perovskite structure doped with metallic ions, *Ceram. Int*. **42 (16)**, 18960-18964 (2016).

[11] Ji, J. H., Shin, D. J., Kim, J. & HyukKoh, J. $BiScO_3$-$PbTiO_3$ piezoelectric ceramics with Bi excess for energy harvesting applications under high temperature. *Ceram. Int.* (2019) https://doi.org/10.1016/j.ceramint.2019.10.117

[12] Meregalli, V. & Savrasov, S. Y. Electron-phonon coupling and properties of doped $BaBiO_3$ *Phys. Rev. B* **57**, 14453-14469 (1998).

[13] Shirai, M., Suzuki, N. & Motizuki, K. Electron-lattice interaction and superconductivity in $BaPb_{1-x}Bi_xO_3$ and $Ba_xK_{1-x}BiO_3$. *J. Phys. Condens. Matter*. **2**, 3553 (1990).

[14] Rubel, M. H. K., Miura, A., Takei, T., Kumada, N., Ali, M. M., Nagao, M., Watauchi, S., Tanaka, I., Oka, K., Azuma, M., Magome, E., Moriyoshi, C., Kuroiwa, Y. & Azharul Islam, A. K. M. Superconducting Double Perovskite Bismuth Oxide Prepared by a Low-Temperature Hydrothermal Reaction, *Angew. Chem. Int. Ed*. **53**, 3599 -3603 (2014).

[15] He, J., Liu, Y. F. & Funahashi, R. Oxide thermoelectrics: The challenges, progress, and outlook. *J. Mater. Res* **26**, 1762-1772 (2011).

[16] Koumoto, K., Funahashi, R., Guilmeau, E., Miyazaki, Y., Weidenkaff, A., Wang, Y., Wan, C., Thermoelectric Ceramics for Energy Harvesting. *J. Am. Ceram. Soc*. **96**, 1-23 (2013).

[17] Srivastava, D., Azough, F., Freer, R., Combe, E., Funahashi, R., Kepaptsoglou, D. M., Ramasse, Q. M., Molinari, M., Yeandel, S. R., Baran, J. D. & Parker, S. C. Crystal structure and thermoelectric properties of Sr-Mo substituted $CaMnO_3$: a combined experimental and computational study. *J. Mater. Chem. C* **3**, 12245-12259 (2015).

[18] Blaha, P., Schwarz, K., Sorantin, P. & Trickey, S. K. Full-potential, linearized augmented plane wave programs for crystalline systems. *Comput. Phys. Commun*. **59**, 339 (1990).

[19] Blaha, P., Schwarz, K., Madsen, G. K. H., Kvasnicka, D. & Luitz, J. WIEN2K, An Augmented Plane Wave + local Orbitals Program for Calculating Crystal Properties, Karl Heinz Schwarz, Techn. Universitat Wien, Austria. 2001.

[20] Tran, F. & Blaha, P. Accurate Band Gaps of Semiconductors and Insulators with a Semi-local Exchange-Correlation Potential. *Phys. Rev. Lett.* **102**, 226401 (2009).

[21] Rakita, Y., Cohen, S. R., Kedem, N. K. & Hodes, G. Mechanical properties of $APbX_3$ (A = Cs or CH_3NH_3; X = I or Br) perovskite single crystals *MRS Communications*, **5**, 623-629 (2015).

[22] Wooten, F. Optical Properties of Solids. Academic Press, New York. 1972.

[23] Madsen, G. K. H., Schwarz, K. & Singh, D. J. BoltzTraP. A code for calculating band-structure dependent quantities. *Comput. Phys. Commun*. **175**, 67 (2006).

[24] Mahmood, Q., Hassan, M. & Noor, N. A. Systematic study of room-temperature ferromagnetism and the optical response of $Zn_{1-x}TM_xS/Se$ (TM = Mn, Fe, Co, Ni) ferromagnets: first-principle approach. *J. Phys.: Condens. Matter*, **28**, 506001 (2016).

[25] Sabir, B., Murtaza, G., Mahmood, Q., Ahmad, R. & Bhamu, K.C. First principles investigations of electronics, magnetic, and thermoelectric properties of rare earth based $PrYO_3$ (Y=Cr, V) perovskites. *Current Appl. Phys*. **17**, 1539-1546 (2017).

[26] Young, J. & Rondinelli, J. Octahedral Rotation Preferences in Perovskite Iodides and Bromides. *Phys. Chem. Lett*. **7**, 918-922 (2016).

[27] Mahmood, Q., Yaseen, M., Haq, B. U., Laref, A. & Nazir, A. The study of mechanical and thermoelectric behavior of $MgXO_3$ (X = Si, Ge, Sn) for energy applications by DFT. *Chem. Phys.* **524**, 106-112 (2019).

[28] Mahmood, Q., Haq, B. U., Yaseen, M., Ramay, S. M., Ashiq, M. G. B. & Mahmood, A. The first-principle study of mechanical, optical and thermoelectric properties of $SnZrO_3$ and $SnHfO_3$ for renewable energy applications. *Solid State Commun.* **292**, 17-23 (2019).

[29] Ji, X., Yu, Y., Ji, J., Long, J., Chen, J. & Liu, D. Theoretical studies of the pressure-induced phase transition and elastic properties of BeS. J. Alloy. *Compd*. **623**, 304 (2015).

[30] Mishra, V., Kumar, A., Sagdeo, A. & Sagdeo, P. R. Comparative structural and optical studies on pellet and powder samples of $BaTiO_3$ near phase transition temperature. *Ceram. Int*. **46**, 3250–3256 (2020). https://doi.org/10.1016/j.ceramint.2019.10.030.

[31] Hassn, M., Shahid, A. & Mahmood, Q. Structural, electronic, optical and thermoelectric investigations of antiperovskites A_3SnO (A = Ca, Sr, Ba) using density functional theory. *Solid State Commun*. **270**, 92-98 (2018).

[32] Hassan, M., Arshad, I. & Mahmood, Q. Semicond. Computational study of electronic, optical and thermoelectric properties of X_3PbO (X = Ca, Sr, Ba) anti-perovskites. *Sci. Technol* **32**, 115002 (2017).

[33] Moghe, D., Wang, L., Traverse, C. J., Redoute, A., Sponsellerb, M., Brown, P. R., Bulovic, V. & Lunt, R. All vapor-deposited lead-free doped $CsSnBr_3$ planar solar cells. *Nano Energy* **28**, 469-474 (2016).

[34] Gupta, S., Bendikov, T., Hodes, G. & Cahen, D. $CsSnBr_3$ A Lead-Free Halide perovskites for Long-Term Solar Cell Application: Insights on SnF_2 Addition. *ACS Energy Lett*. **5,** 1028-1033 (2016).

[35] Gupta, S., Bendikov, T., Hodes, G. & D. Cahen, $CsSnBr_3$, A Lead-Free Halide Perovskites for Long-Term Solar Cell Application: Insights on SnF_2 Addition. *ACS Energy Lett*. **1,** 1028-1033 (2016).

[36] Cao, P., Yang, B., Zheng, F., Wang, L. & Zou, J. High stability of silica-wrapped $CsPbBr_3$ perovskite quantum dots for light emitting application. *Ceram. Int.* **46**, 3882–3888 (2020). https://doi.org/10.1016/j.ceramint.2019.10.114

[37] Jiang, S., Fang, Y., Li, R., Xiao, H., Crowley, J., Wang, C., White, T. J., Goddard III, W.A., Wang, Z., Baikie, T. & Fang, J. Pressure-Dependent Polymorphism and Band-Gap Tuning of Methyl ammonium Lead Iodide perovskites. *Angew. Chem. Int. Ed* **55**, 6540 (2016).

[38] Haq, B. U., AlFaify, S., Laref, A., Ahmed, R., Butt, F. K., Chaudhry, A. R., Ur Rehman, S. & Mahmood, Q. Optoelectronic properties of new direct bandgap polymorphs of single-layered Germanium sulfide. *Ceram. Int.* **45**, 18073-18078 (2019).

[39] Noor, N. A., Mahmood, Q., Rashid, M., Haq, B. U. & Laref, A. The pressure-induced mechanical and optoelectronic behavior of cubic perovskite $PbSnO_3$ via ab-initio investigations. *Ceram. Int.* **44**, 13750-13756 (2018).

[40] Mahmood, Q., Ashraf, A. & Hassan, M. Investigations of optical and thermoelectric response of direct band gap Ca_3XO (X = Si, Ge) anti-perovskites stabilized in cubic and orthorhombic phases. *Indian J. Phys*. **92**, 865-874 (2018).

[41] Penn, D. R. Wave-Number-Dependent Dielectric Function of Semiconductors. *Phys. Rev*. **128**, 2093 (1962).

[42] Cai, M., Yin, Z. & Zhang, M. First-principles study of optical properties of barium titanate. *Appl. Phys. Lett*. **83**, 2805 (2003).

[43] Zhang, Y., Li, L., Bai, W., Shen, B., Zhai, J. & Li, B. Effect of $CaZrO_3$ on phase structure and electrical properties of KNN-based lead-free ceramics. *RSC Adv*. **5**, 19647-19651 (2015).

[44] Madsen, G. K. H. & Singh, D. J. BoltzTraP. A code for calculating band-structure dependent quantities. *Comput. Phys. Commun* **175**, 67-71 (2006).

[45] Murtaza, G. & Ahmad, I. First principle study of the structural and optoelectronic properties of cubic perovskites CsPbM3 (M = Cl, Br, I). *Physica. B* **406**, 3222-3229 (2011).

[46] Reshak, A. H., Khan, S. A. & Auluck, S. Thermoelectric properties of a single graphene sheet and its derivatives. *J. Mater. Chem. C* **2**, 2346-2352 (2014).

[47] Reshak, A. H. & Auluck, S. Thermoelectric properties of Nowotny-Juza NaZnX (X= P, As and Sb) compounds. *Compute. Mater. Sci.* **96**, 90-95 (2015).

[48] Toshio, M. Y., Uedahiroshi, K. K. & Hosono, Y. H. High-temperature thermoelectric properties of La-doped $BaSnO_3$ ceramics. *Mater. Sci. Eng. B* **173**, 29-32 (2010).

[49] Zhao, D., Chen, J., Ren, Z., Chen, J., Song, Q. F., Zhang, Q., Chen, N. & Jiang, Y. Thermoelectric transport and magnetoresistance of electrochemical deposited Bi_2Te_3 films at micrometer thickness. *Ceram. Int.* **46**, 3339-3344 (2019).

[50] Khan, Tahsin, T. & Chul, U. S. Thermoelectric Properties of the perovskites-Type Oxide $SrTi_{1-x}Nb_xO_3$ Synthesized by Solid-State Reaction Method. *Electron. Mater. Lett.* **14**, 336-341 (2018).

[51] Oyama, T., Muta, H., Uno, M. & Yamanaka, S. Thermoelectric properties of perovskites type barium molybdate. *J. Alloy Compd.* **372**, 65-69 (2004).

[52] Varshni, Y. P.Temperature dependence of the energy gap in semiconductors. *Physica* **34**, 149-154 (1967).

[53] Bhamu, K.C., Soni, A. & Sahariya, J. Revealing optoelectronic and transport properties of potential perovskites Cs_2PdX_6 (X = Cl, Br): A probe from density functional theory (DFT). S*ol. Energy* **162**, 336-343 (2018).